(Preprint) AAS 23-284

MISSION DESIGN FOR NEAR-FUTURE SOLAR POLAR IMAGING MISSION LEVERAGING VENUS FLYBY

James B. Pezent[*], Rohan Sood[†], Andrew Heaton[‡] and Les Johnson[§]

In this work, trajectory design scenarios for near future solar polar imaging missions leveraging solar sails are examined. Specifically,investigatation is carried out to explore whether including a Venus flyby can improve the overall mission time of flight compared to a traditional SPI mission architecture. For both the flyby and non-flyby architectures, time optimal transfers are computed to a 75° inclination science orbit at 0.48 AU across a range of feasible Earth departure energies, cranking radii, and sail sizes. Preliminary results suggest that including a Venus flyby reduces overall mission time of flight by 12-17% compared to the traditional mission architecture.

INTRODUCTION

The heliophysics community has long sought to observe the Sun from highly inclined vantage points. Viewing the solar polar regions will allow insights into solar magnetic field interactions that drive much of solar activity, including helioseismology observations from a high latitude, measurements of the photospheric magnetic fields in the polar regions, and direct measurements of the heliospheric magnetic field and solar wind.[1] The high latitude also gives the spacecraft a unique top-down view of coronal mass ejections (CMEs) that could affect space weather around Earth and allow the velocity and directions of these CMEs to be better quantified.[1]

Unfortunately, reaching even moderate heliocentric inclinations is challenging using traditional propulsion systems, owing to large fuel requirements and long mission times. To date, the Ulysses mission is the only mission that provided a vantage point from outside the ecliptic plane.[2] Because of the long period orbits necessitated by the Jupiter gravity assist to achieve a highly inclined solar orbit, Ulysses made only 3 orbits (3 passes above north and south poles of the Sun respectively).[2] The solar polar regions are not observable from Earth or spacecraft flying in or near the ecliptic plane. As such, solar sails have been proposed as a promising option for reaching highly inclined solar obits. Solar sail technology is uniquely capable of reaching the lower solar altitude and higher solar inclination required for solar polar imaging missions because thrust increases as the solar distance reduces. Electric propulsion can achieve some efficiencies due to greater power available as solar distance is reduced, but the effect is not as direct as the inverse square effect of closer distance to the Sun that photonic propulsion can achieve.

Beginning in earnest with the original Solar Polar Imager (SPI) concept,[3] numerous sail-based solar polar imaging missions have been proposed and studied in detail.[1,4,5] Common to most of these studies is the requirement that the spacecraft inserts itself into a 0.48 AU radius science orbit inclined at least 75° with respect to the ecliptic plane. An orbit with these properties would be in 3:1 resonance with Earth, enabling

[*]PhD Candidate, Astrodynamics and Space Research Laboratory, The University of Alabama, 245 7th Ave., Tuscaloosa, AL 35487, jbpezent@crimson.ua.edu.

[†]Associate Professor, Astrodynamics and Space Research Laboratory, The University of Alabama, 245 7th Ave., Tuscaloosa, AL 35487, rsood@eng.ua.edu.

[‡]Senior Aerospace Engineer, EV/42, NASA Marshall Space Flight Center, NASA Marshall Space Flight Center, Huntsville, AL 35812, andrew.f.heaton@nasa.gov.

[§]Solar Sail PI, Science and Technology Office, NASA Marshall Space Flight Center, NASA Marshall Space Flight Center, Huntsville, AL 35812, les.johnson@nasa.gov.

uninterrupted communication, while also allowing for sufficient time at high solar latitudes to observe relevant phenomena.[3]

BACKGROUND AND OBJECTIVE

Early SPI solar sail mission design studies focused on computing time optimal transfers directly from Earth to the target science orbit. These transfers are roughly broken down into two phases: a spiral to the science orbit radius, and then cranking inclination to the desired value at this radius. In general, the majority of the transfer time is spent in the inclination cranking phase. Previous studies have conclusively shown that the duration of the inclination cranking phase can be reduced by selecting a smaller science orbit radius.[6] This is due to the fact that a solar sail's rate of inclination change is inversely proportional to the period of the cranking orbit. However, the typical science orbit radius of 0.48 AU in SPI mission concepts is driven by science, instrumentation, and communications considerations, and cannot be chosen to minimize total mission time of flight (TOF). Therefore, as a simple method to improve TOF, studies[6–8] have investigated breaking down the mission into 3 phases. In the first phase, one departs Earth and spirals down to a circular cranking orbit with a radius less than the desired science orbit. In the second phase, the sail then executes the inclination cranking maneuver at this smaller radius in a shorter amount of time. After reaching the desired inclination, in the final phase, the sail-craft then performs a co-planar transfer to raise itself into a circular science orbit at 0.48 AU. This mission architecture, in this work termed standard SPI, has been examined in depth by Macdonald[8] and Dachwald.[7] It was found that the resulting reduction in the length of the inclination cranking phase exceeded the additional time necessary to spiral below and then return to the science orbit, resulting in significant improvements in overall TOF across all examined sail sizes. Mengali and Quarta investigated this mission architecture further and conclusively showed that there is a maximum terminal inclination of approximately 20°, beyond which the 3 phase transfer is the superior option.[9] As the first step in this work, a process to generate near optimal 3 phase standard SPI transfers is developed. These are then used to seed the construction of fully optimal standard SPI transfers that go directly from Earth to the target orbit while maintaining a minimal distance from the Sun.

Next, it is investigated whether the inclusion of a single Venus flyby during the spiral down will further improve overall mission time of flight. McDonald[8] and Appourchaux[4] both observed modest improvements leveraging Venus gravity assists for point solutions, but it remains to be seen whether this holds true across the whole parameter space. However, Quarta and Mengali found that including a Venus flyby can significantly reduce TOF for solar sail missions to Mercury[10] across a wide range of sail sizes. Considering the similarity between the radius of Mercury's orbit and commonly considered SPI cranking orbits, it is reasonable to assume that a Venus flyby could benefit SPI missions in a similar manner. To answer this definitively, a simple method to construct near optimal 4 phase Venus flyby SPI transfers is developed. Similar to the standard SPI case, near optimal solutions are used as initial guesses in the construction of fully optimal Venus flyby SPI transfers. The performance of both optimal mission architectures are then compared across a range of sail-sizes, cranking radii, and Earth departure energies.

DYNAMICAL MODELLING

To facilitate the optimization of multi-revolution solar sail trajectories, the Sun-centered two-body dynamics are expressed in modified equinoctial elements (MEEs).[11] Work by Junkins and Taheri has shown that formulating and solving low-thrust optimization problems in MEEs can be significantly faster and more robust than alternative representations.[12] In MEEs, the state of the spacecraft is parameterized using the six state variables, $\vec{X}$, only two of which, p (semi-latus rectum) and L (true longitude), have a straightforward physical interpretation (eq. (1)). The controls, $\vec{U}$, for the sail-based model are the unit normal vector of the sail, $\hat{n}$, expressed in the radial-tangential-normal (RTN) frame.

$$\vec{X} = [p, f, g, h, k, L]^T \quad ; \quad \vec{U} = \hat{n} = [n_r, n_t, n_n]^T \tag{1}$$

The equations of motion can be written in compact matrix notation as the product of matrix, $\mathbf{A}(\vec{X})$, and sail-induced acceleration, $\vec{a}_s(\vec{X}, \vec{U})$, plus a vector $\vec{b}(\vec{X})$ which contains the unperturbed two-body dynamics

of L.

$$\dot{\vec{X}} = \mathbf{A}\vec{a}_s + \vec{b} \tag{2}$$

The matrix, $\mathbf{A}(\vec{X})$, and vector, $\vec{b}(\vec{X})$, can be computed using eq. (3) below. Common sub expressions w and s^2 appearing in eq. (3) are given by eq. (4).

$$\mathbf{A} = \sqrt{\frac{p}{\mu}} \begin{bmatrix} 0 & \frac{2p}{w} & 0 \\ \sin L & \frac{1}{w}[(w+1)\cos L + f] & -\frac{g}{w}[h\sin L - k\cos L] \\ -\cos L & [(w+1)\sin L + g] & \frac{f}{w}[h\sin L - k\cos L] \\ 0 & 0 & \frac{s^2\cos L}{2w} \\ 0 & 0 & \frac{s^2\sin L}{2w} \\ 0 & 0 & [h\sin L - k\cos L] \end{bmatrix}$$
$$\vec{b} = [0, 0, 0, 0, 0, \sqrt{\mu p}\frac{w^2}{p^2}]^T \tag{3}$$

$$\begin{aligned} w &= 1 + f\cos L + g\sin L \\ s^2 &= 1 + h^2 + k^2 \end{aligned} \tag{4}$$

Solar sail acceleration is modeled using the non-ideal McCinnes sail model (eq. (5)) with optical coefficients derived from empirical testing of NEA Scout's aluminized mylar sail material.[13–16] Sail-size/thrust is characterized by the ideal sail lightness parameter, β, which is simply the ratio of acceleration induced by a perfectly reflecting surface to the acceleration due to the Sun's gravity at 1 AU.

$$\vec{a}_s = \frac{\beta}{2}\frac{\mu}{r^2}\left((n_1\cos^2(\alpha) + n_2\cos(\alpha))\,\hat{n} + (t_1\cos(\alpha)\sin(\alpha))\hat{t}\right) \tag{5}$$

The instantaneous distance from the Sun, r, and terms involving the sail incidence angle, α, and sail unit tangent vector, $\hat{t}$, can be expressed in terms of the MEEs and the sail's normal vector as shown below.

$$r = \frac{p}{w} \quad ; \quad \cos(\alpha) = n_r \quad ; \quad \sin(\alpha)\hat{t} = [n_t^2 + n_n^2, -n_r n_t, -n_r n_n]^T \tag{6}$$

Constants n_1, n_2, and t_1 capture the non-ideal behavior of the sail are derived from the reflectivity ($\tilde{\mathbf{r}}$), specular ($\mathbf{s}$), and front/back emisivity ($\mathbf{e_{f,b}}$) and Lambertian ($\mathbf{B_{f,b}}$) coefficients of NEA Scout's sail material shown in table 1.

$$n_1 = 1 + \tilde{\mathbf{r}}\tilde{\mathbf{s}} \quad ; \quad n_2 = \mathbf{B_f}(\mathbf{1} - \tilde{\mathbf{s}})\tilde{\mathbf{r}} + (\mathbf{1} - \tilde{\mathbf{r}})\left(\frac{\mathbf{e_f}\mathbf{B_f} - \mathbf{e_b}\mathbf{B_b}}{\mathbf{e_f} + \mathbf{e_b}}\right) \quad ; \quad t_1 = 1 - \tilde{\mathbf{r}}\tilde{\mathbf{s}}$$

To improve the numerical conditioning of eq. (3), canonical units are employed by setting $\mu = 1$. In this unit

Table 1: NEA Scout Optical Coefficients

$\tilde{\mathbf{r}}$	$\tilde{\mathbf{s}}$	$\mathbf{B_f}$	$\mathbf{B_b}$	$\mathbf{e_f}$	$\mathbf{e_b}$
0.91	0.89	0.79	0.67	0.025	0.27

system, the non-dimensional length scale is 1 AU and 2π non-dimensional time units is equal to 1 year.

While it is best to represent low-thrust dynamics in MEEs, certain constraints and objectives employed in later sections are more easily represented in standard Cartesian coordinates and classical orbital elements. Transformation from MEEs to the Cartesian position, $\vec{r}$, and velocity, $\vec{v}$, relative to the Sun can be accomplished with eq. (7).[17]

$$
\begin{aligned}
\vec{r} &= \begin{bmatrix} \frac{r}{s^2}\left(\cos L + \sigma^2 \cos L + 2hk \sin L\right) \\ \frac{r}{s^2}\left(\sin L - \sigma^2 \sin L + 2hk \cos L\right) \\ \frac{2r}{s^2}\left(h \sin L + k \cos L\right) \end{bmatrix} \\
\vec{v} &= \begin{bmatrix} -\frac{1}{s^2}\sqrt{\frac{\mu}{p}}\left(\sin L + \sigma^2 \sin L - 2hk \cos L + g - 2fhk + \sigma^2 g\right) \\ -\frac{1}{s^2}\sqrt{\frac{\mu}{p}}\left(-\cos L + \sigma^2 \cos L + 2hk \sin L - f + 2ghk + \sigma^2 f\right) \\ \frac{2}{s^2}\sqrt{\frac{\mu}{p}}\left(h \cos L + k \sin L + fh + gk\right) \end{bmatrix} \\
\sigma^2 &= h^2 - k^2
\end{aligned}
\tag{7}
$$

Additionally, the classical orbital elements can be calculated directly from the MEEs using eq. (8).

$$
\begin{aligned}
a &= \frac{p}{1 - f^2 - g^2} \\
e &= \sqrt{f^2 + g^2} \\
i &= 2 \arctan\left(\sqrt{h^2 + k^2}\right) \\
\omega &= \arctan(gh - fk, fh + gk) \\
\Omega &= \arctan(k, h) \\
\theta &= L - \arctan(g/f)
\end{aligned}
\tag{8}
$$

TRANSFER DESIGN

The Astrodynamics Software and Science Enabling Toolkit (ASSET), developed at the University of Alabama, is used to formulate and solve all optimization problems in this work.[18] ASSET employs a direct collocation scheme to transcribe optimal control problems into sparse non-linear programs that are solved using the built-in optimizer PSIOPT. Exact first and second derivatives for all constraints, objectives, and dynamics are computed using ASSET's automatic/analytic differentiation capabilities and accelerated with a combination of AVX-2 vectorization and multi-threading.

Standard SPI

For SPI type missions, one seeks to minimise total transfer time from Earth to a highly inclined science orbit at 0.48 AU. Earth departure C_3 should be constrained to reflect the capabilities of the launch vehicle. However, with no further constraints, the optimal transfer would have the sail spiral down to exactly zero radius to perform the inclination cranking maneuver 'instantaneously' before spiraling back up to 0.48 AU, which, while although optimal, is not physically possible. Thus, one needs to place a lower bound on the minimum allowable distance from the Sun during the transfer. With this constraint, the problem is well posed, and can be solved as a single phase optimal control problem. However, finding such multi-revolution low-thrust transfers can be challenging without a good initial guess, even with an appropriate choice of coordinates. Therefore, in this work, a multi-step approach of first computing near time optimal transfers to the target orbit before tackling the full problem is adopted. These transfers are divided into 3 distinct phases similar to many previous studies.

1. Depart Earth with some allowable C_3 , deploy sail, and spiral to a cranking radius, $a_{crank} < 0.48$ AU.
2. Crank inclination to 75° at a constant radius of a_{crank}.
3. Raise orbit to nominal science orbit radius of 0.48 AU.

First, for a given sail lightness parameter, β, and upper bound on Earth departure C_3, the construction of phase 1 begins with computing a time optimal planar transfer from Earth to a circular orbit at a minimum

cranking radius, a_{crank}. Since the standard SPI architecture considered in this work is agnostic to launch date, it is always assumed that the Earth is in a planar 1 AU circular orbit and that the sail-craft starts on the positive x-axis. In non-dimensional units, the constraints on Earth departure (eq. (9)) are expressed in Cartesian coordinates leveraging eq. (7).

$$\vec{r}(\vec{X}(0)) - [1,0,0]^T = \vec{0} \quad |\vec{v}(\vec{X}(0)) - [0,1,0]^T|^2 \leq C_3 \tag{9}$$

Enforcing arrival in a circular orbit of radius a_{crank} can specified as shown eq. (10).

$$[p(t_f), f(t_f), g(t_f)]^T - [a_{crank}, 0, 0]^T = \vec{0} \tag{10}$$

As an initial guess for this sub-problem problem, it is generally sufficient to integrate the equations of motion with a constant 35° retrograde incidence angle until the sail crosses the target orbit radius, a_{crank}.

Optimized solutions to the planar time-optimal problem are then provided as the initial guess for the solution of phase 1, which aims to maximize the inclination of the terminal circular orbit at a_{crank}. An upper bound is placed on the final time that is 20% longer than the optimum planar transfer time. This strategy allows us to compute a phase 1 spiral-down transfer that leverages the Earth departure C_3 for both radius and inclination change, without having to consider the entire inclination cranking phase. In practice, the maximal terminal inclination achieved in this time window is only 10° - 30°, far less than the 75° requirement. An initial guess for the remainder of the orbit cranking phase (phase 2) is computed using the analytic control law for maximal solar sail inclination change as shown in eq. (11). The control law aligns the normal vector of the sail to produce maximum acceleration in the normal direction of the RTN frame, and switches direction twice per orbit so as to always increase the current inclination. For the sail model considered in this paper, normal acceleration is maximized by setting the incidence angle, $\alpha = 35.4°$.

$$\hat{n} = [\cos(\alpha), 0, \text{sgn}\left(\frac{h\cos L + k\sin L}{w}\right) * \sin(\alpha)] \tag{11}$$

The cranking phase is then optimized to reach the 75° target inclination from the fixed state at the end of phase 1 in minimum time, subject to a lower bound of a_{crank} on the minimum distance from the Sun.

Upon reaching the desired inclination, phase 3 is computed by finding the time-optimal transfer from the fixed state at the end of the orbit cranking phase to a co-planar science orbit at 0.48 AU. Similar to phase 1, to generate an initial guess for this problem, it is sufficient to integrate out the final state of the inclination cranking phase with a 35° prograde incidence angle until it crosses the 0.48 AU science orbit radius. When solved and combined with phases 1 and 2, a continuous near time-optimal transfer from Earth to the target science orbit at the desired inclination is achieved. As an example, this process is applied for $\beta = .04$, $a_{crank} = .35AU$, and $C_3 = 12\frac{km^2}{s^2}$. A β value of .04 represents a sail twice as large as Solar Cruiser,[14] and is a conservative estimate for the performance of next generation solar sails. The resulting transfer shown in fig. 1 has a total TOF of 7.528 years (2747 days), which is itself not unreasonable compared to many previous high-value science missions

Time of flight can then be further improved by optimizing the entire trajectory end-to-end as a single phase subject to departure conditions eq. (9), a path constraint specifying a minimum distance from the Sun of a_{crank}, and terminal constraints specifying arrival in a 75° inclination circular orbit at 0.48 AU. Applying this process to the previous example results in a fully optimal standard SPI transfer (fig. 2) with total TOF of 7.339 years (2679 days), a 68 day improvement over the near time-optimal transfer.

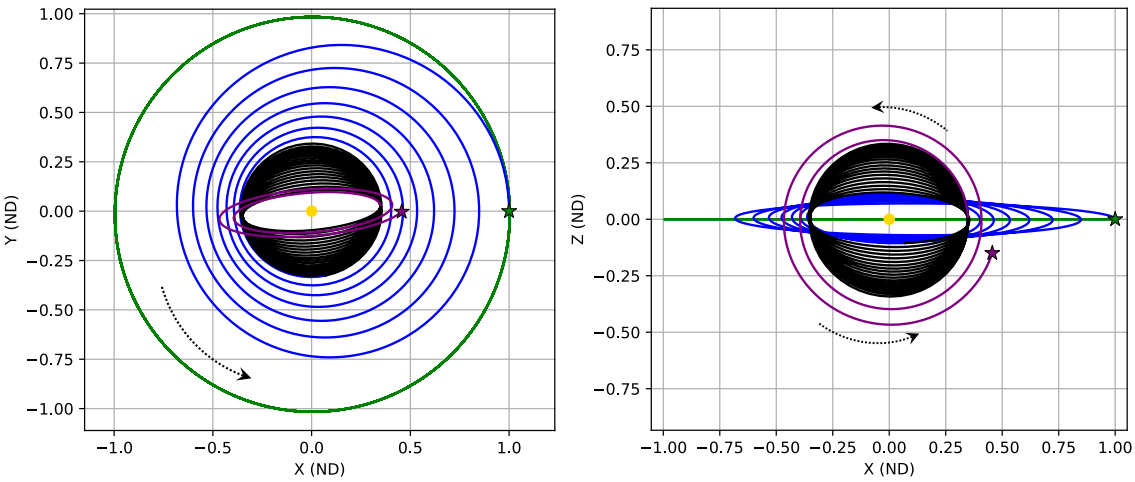

(a) (b)

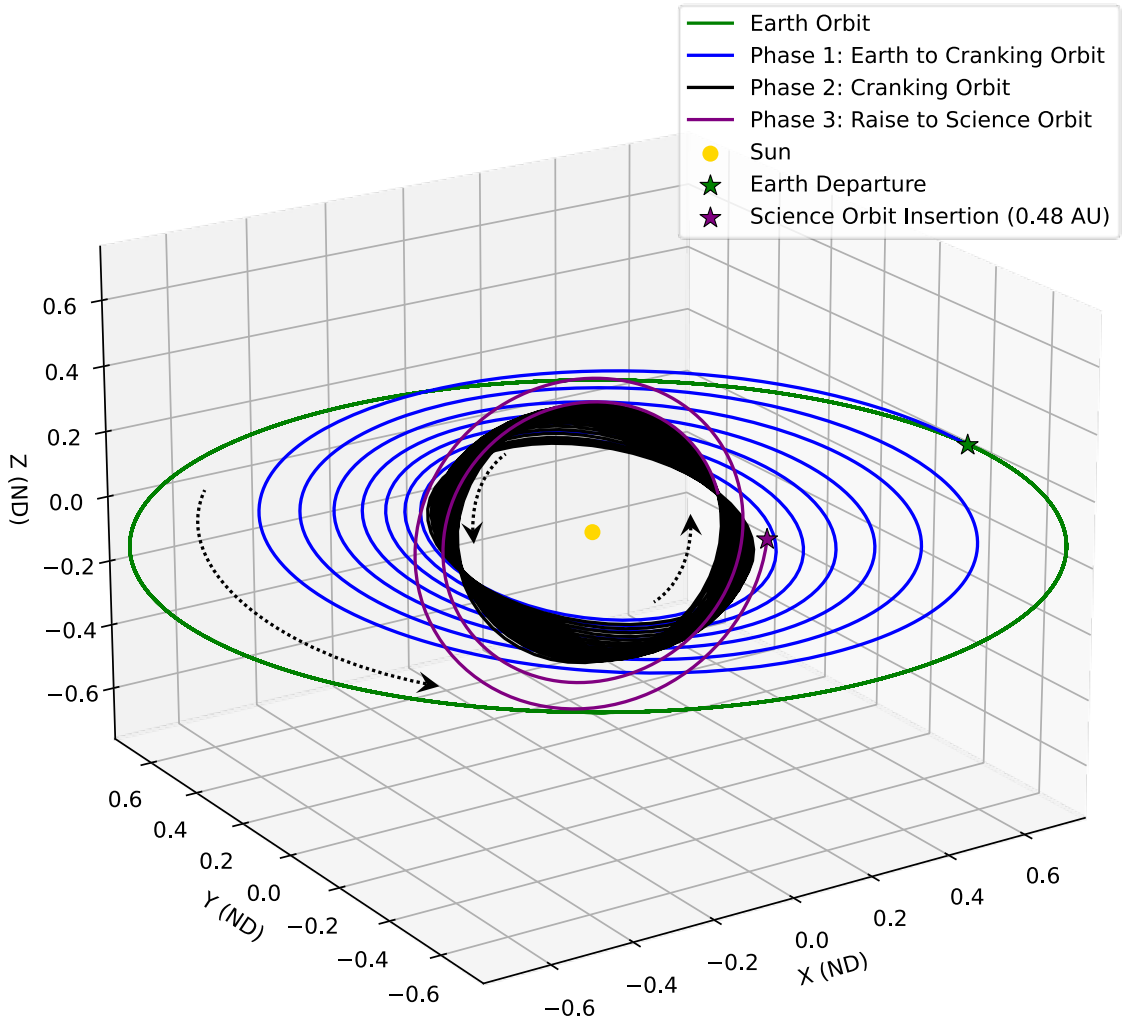

(c)

Figure 1: Near Optimal Standard SPI: (a) X-Y View; (b) X-Z View; (c) 3D View;

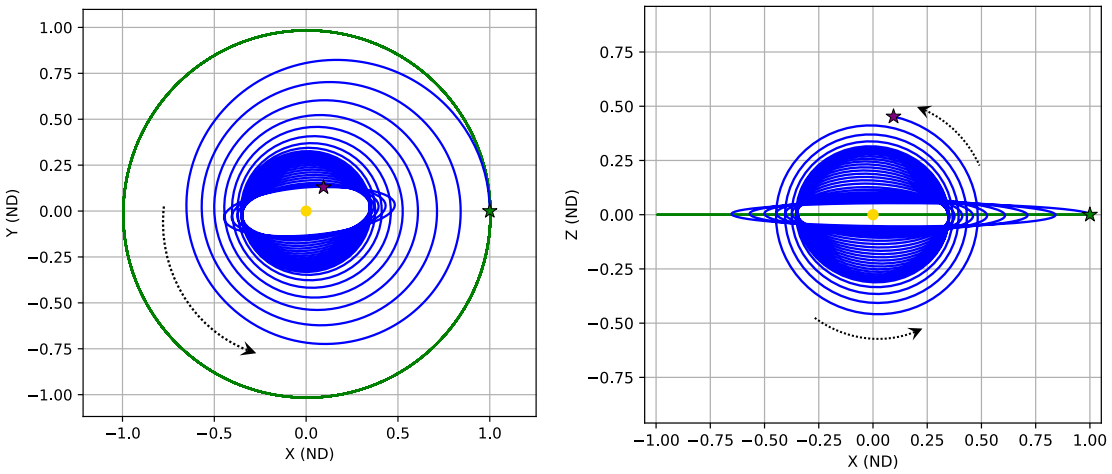

(a) (b)

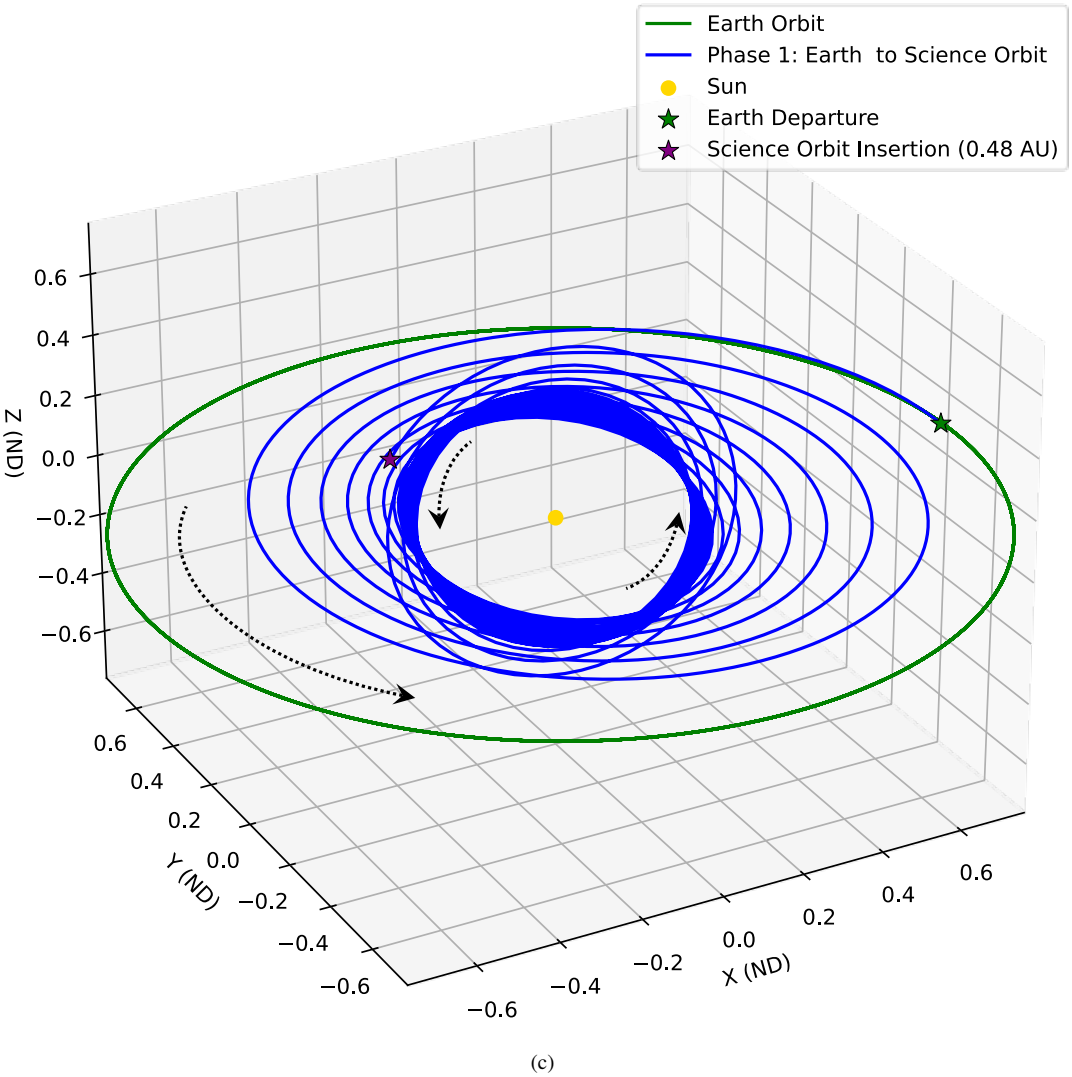

(c)

Figure 2: Optimal Standard SPI: (a) X-Y View; (b) X-Z View; (c) 3D View;

Venus Flyby SPI

Construction of time-optimal Venus flyby transfers proceeds in a similar multi-step fashion as the standard SPI architecture, except that the initial near-optimal transfer is broken down into 4 distinct phases.

1. Depart Earth with some allowable C_3, deploy sail, and flyby Venus.
2. Spiral to a cranking radius, $a_{crank} < 0.48$ AU, with inclination change.
3. Crank inclination to 75° at a constant radius of a_{crank}.
4. Raise orbit to nominal science orbit radius of 0.48 AU.

To properly leverage Earth departure C_3 and the Venus flyby to minimize total TOF, phase 1 ($X_1(t)$) and phase 2 ($X_2(t)$) are optimized together. The constraint on the Earth departure at the beginning of phase 1 is formulated by converting MEEs into Cartesian coordinates and relating them to the time-dependent heliocentric position, $\vec{r}_e$, and velocity, $\vec{v}_e$, of the Earth as calculated using the DE 432 ephemeris. Note the Earth departure time, t_e, is allowed to vary freely.

$$\vec{r}(\vec{X}_1(t_e)) - \vec{r}_e(t_e) = \vec{0} \quad ; \quad |\vec{v}(\vec{X}_1(t_e)) - \vec{v}_e(t_e)|^2 \leq C_3 \tag{12}$$

To model the flyby separating the end of phase 1 and beginning of phase 2, the zero sphere of influence flyby approximation is employed. This can be modeled by first enforcing that both phases encounter Venus at common flyby time, t_v. For simplicity, the inbound, V_∞^-, and outbound, V_∞^+, relative velocity magnitudes at Venus are also constrained to be equal. Thus, the effects of sail thrust within Venus's sphere of influence are being ignored, or alternatively it is assumed that the sail is turned edge on to the Sun during the flyby.

$$\begin{gathered}\vec{r}(\vec{X}_1(t_v)) - \vec{r}_v(t_v)^T = \vec{0} \quad ; \quad \vec{r}(\vec{X}_2(t_v)) - \vec{r}_v(t_v)^T = \vec{0} \quad ; \quad |V_\infty^-| = |V_\infty + | \\ \text{where} \\ |V_\infty^-| = |\vec{v}(\vec{X}_1(t_v)) - \vec{v}_v(t_v)| \quad ; \quad |V_\infty^+| = |\vec{v}(\vec{X}_2(t_v)) - \vec{v}_v(t_v)|\end{gathered} \tag{13}$$

The turning angle, Δ, induced by the flyby is then bounded to be less than the maximum turning angle, Δ_{max}, commensurate with the arrival/departure V_∞, Venus's gravitational parameter, μ_v, and a minimum allowable flyby radius, R_{min}. In this work, a minimum flyby radius of 6500 km is assumed, which is equivalent to a 450 km minimum flyby altitude.

$$\begin{gathered}\Delta \leq \Delta_{max} \\ \Delta = \arccos\left(\hat{V}_\infty^+ \cdot \hat{V}_\infty^-\right) \quad ; \quad \Delta_{max} = 2 * \arcsin\left(\frac{\mu_v}{\mu_v + R_{min} V_\infty^2}\right)\end{gathered} \tag{14}$$

Finally, at then end of phase 2, arrival at a_{crank} is enforced using eq. (10).

In contrast to the previous section, for the Venus flyby architecture, the strategy directly optimizes terminal inclination at a_{crank} in fixed time rather than first finding a time-optimal planar transfer. This strategy produced overall solutions with marginally better TOF. For the combined problem, phase 1 is initialized with the minimum ΔV Lambert solution from Earth to Venus within a predefined launch and arrival window. Phase 2's initial guess is then generated by integrating the equations of motion from Venus's state at the flyby with a shallow 25° retrograde incidence angle until the sail reaches a_{crank}. The upper bound on total TOF is taken to be 10% longer than the initial guess.

After computing an optimal solution to phases 1 and 2, the computation of the rest of the cranking phase and orbit-raising phase proceeds identically to that described in the previous section. As a direct comparison with the standard SPI, fig. 3 illustrates the near optimal solution for $\beta = .04$, $a_{crank} = .35$ AU, and $C_3 = 12\frac{km^2}{s^2}$. The departure date range was constrained to lie between January 1, 2030 and January 1, 2032. The fully optimized solution departs Earth on June 10, 2031 and performs the Venus flyby on November 21, 2031

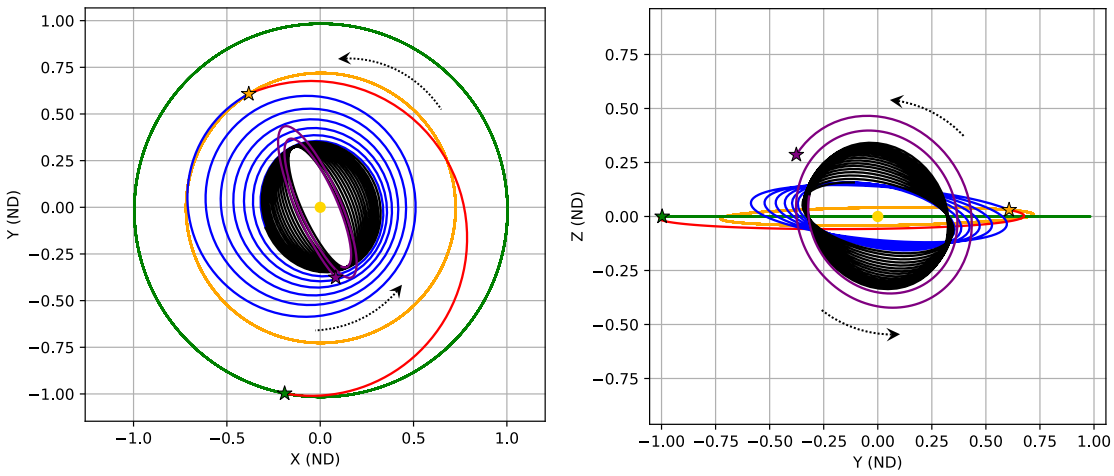

(a) (b)

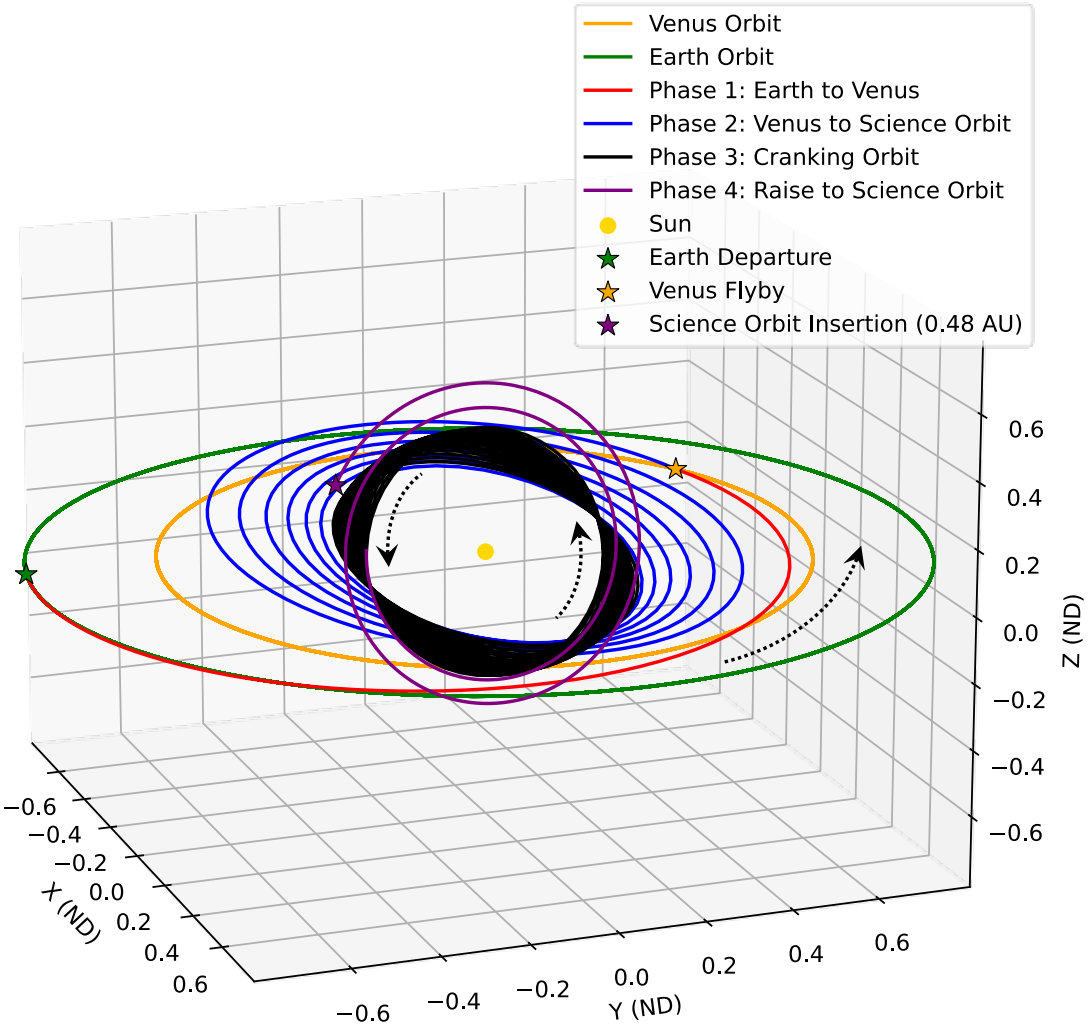

(c)

Figure 3: Near Optimal Venus Flyby SPI: (a) X-Y View; (b) Y-Z View; (c) 3D View;

before arriving in the target orbit on December 5, 2037. Overall TOF is 6.492 years (2369 days), 309 days faster than the equivalent fully optimized standard SPI mission.

Given a near optimal Venus flyby SPI trajectory, the entire trajectory to the 75° science orbit end-to-end is optimized to obtain a fully optimal solution. This problem consists of two phases (Earth to Venus and Venus to science orbit) that are optimized together. The initial guess for the first phase is taken to be the first phase of the near optimal transfer. The second phase is the concatenation of phases 2 through 4 from the near optimal solution. Solving this problem for the previous example results in the transfer shown in fig. 4. Total TOF is reduced to 6.147 years (2243 days), a 442 day or 16.25% improvement over the equivalent fully optimal standard SPI mission.

The parameters of the example Venus flyby mission architectures are summarized below in table 2. Both trajectories depart Earth and arrive at Venus on similar dates, which is unsurprising considering that the optimal solution is initialized with the near optimal one. Also unsurprising is that both trajectories fly by Venus at the minimum allowable radius to maximize energy gain during the encounter. What is interesting however, is that for the optimal trajectory, the Venus flyby imparts a smaller inclination change on the spacecraft, but results in a larger reduction in semi-major axis. This suggest that there is some trade-off between leveraging the flyby to directly increase inclination and leveraging it to reach the cranking radius faster.

Table 2: Parameters of Venus flyby mission architectures for $\beta = .04$, $a_{crank} = .35$ AU, and $C_3 = 12\frac{km^2}{s^2}$.

	Near Optimal Venus Flyby	Optimal Venus Flyby
Departure Date	6-10-2031	6-14-2031
Venus Flyby Date	11-21-2031	11-20-2031
Arrival Date	12-5-2037	8-4-2037
Total TOF	6.492 years, 2369 days	6.147 years, 2243 days
Improvement over Standard SPI	309.5 days, 11.55%	425.4 days, 16.25%
Venus Flyby Radius	6500 km	6500 km
Flyby Δi	6.695°	5.579°
Flyby Δa	-0.207 AU	-.2257 AU

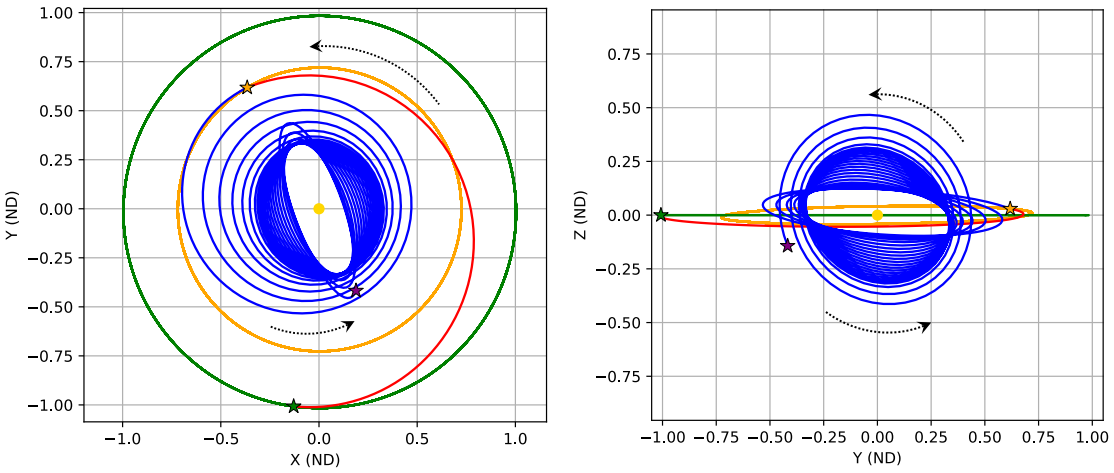

(a) (b)

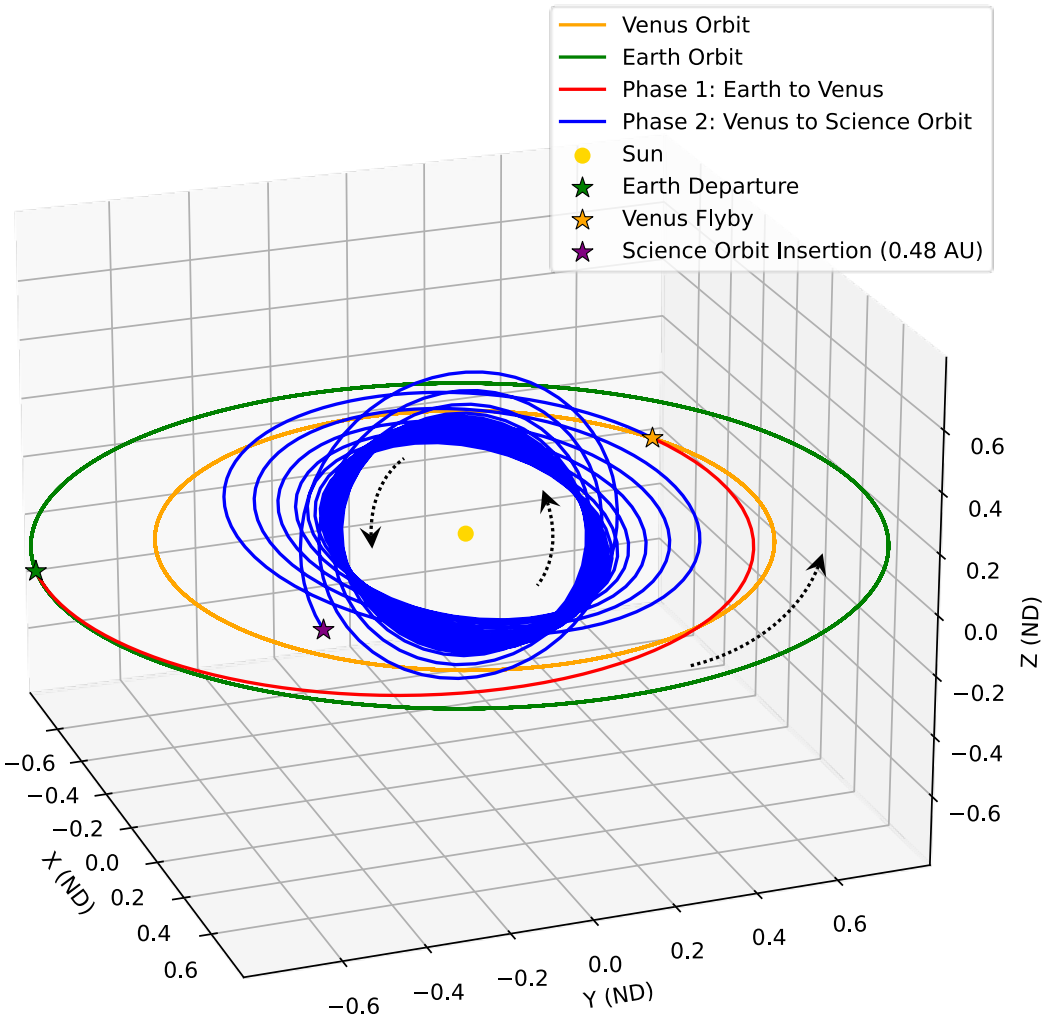

(c)

Figure 4: Optimal Venus Flyby SPI: (a) X-Y View; (b) Y-Z View; (c) 3D View;

TRADE STUDY

Leveraging the trajectory design strategy described in the previous sections, a trade study is run to establish the relative performance of the optimal Standard and optimal Venus flyby SPI mission architectures across a range of β and a_{crank}. For this work, a_{crank} values ranging from 0.45 AU to 0.25 AU and β ranging 0.02 to 0.06 are examined. The lower limit on β is representative of the current state of the art in solar sail manufacturing (Solar Cruiser[14,15]) and the upper limit roughly encompasses the maximum performance that Marshall Space Flight Center projects for next generation solar sails. Consistent with the previous examples, departure dates for the Venus flyby SPI transfers are constrained to lie between January 1, 2030 and January 1, 2032.

As a first trade, Earth departure C_3 is set to a moderate $12\frac{km^2}{s^2}$, roughly comparable to that required for traditional missions to Venus or Mars. The optimal TOF for the standard and Venus flyby SPI mission architectures across this trade space are computed and represented as a contoured heat maps in fig. 5 and fig. 6, respectively. For reference, the previous examples for $\beta = .04$ and $a_{crank} = 0.35$ AU occur at the precise center of each plot. Starting with the standard SPI architecture in fig. 5 and scanning left to right at constant values of a_{crank}, it is apparent that overall mission TOF is reduced roughly inversely proportional to sail β value as one would expect. Most importantly though, at constant β value, performing the inclination cranking maneuver at smaller a_{crank} always improves overall mission TOF. Thus, as noted by Dachwald,[7] in order to minimize the time of flight for the standard SPI mission architecture, the inclination cranking maneuver should be performed at the smallest radius allowable by thermal limits on the spacecraft. The results of the TOF trade study for the Venus flyby mission architecture are shown in fig. 6. The same general trends and conclusions seen for the standard SPI regarding β and a_{crank} hold here as well, with lower cranking radii always improving the TOF.

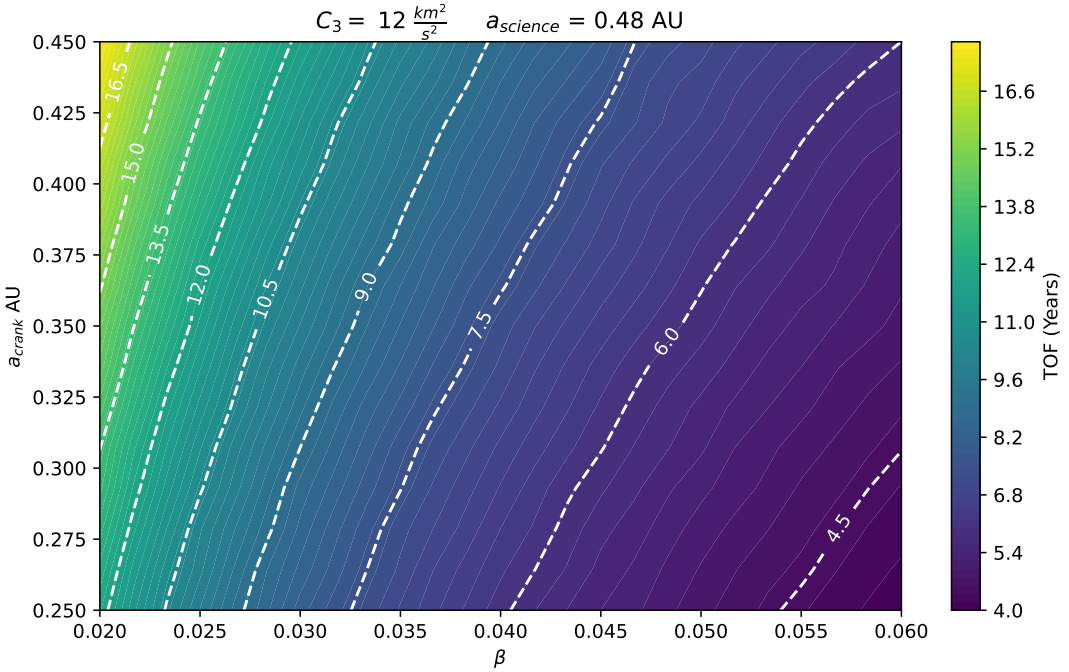

Figure 5: Overall TOF for Optimal Standard SPI Architecture, $C_3 = 12\ \frac{km^2}{s^2}$

For a more direct comparison, fig. 7 shows the percentage improvement in the TOF due to the Venus flyby across the trade space. Note, one should not expect fig. 7 to be completely smooth considering that the optimal Venus flyby architecture is computed using boundary conditions derived from ephemeris data and

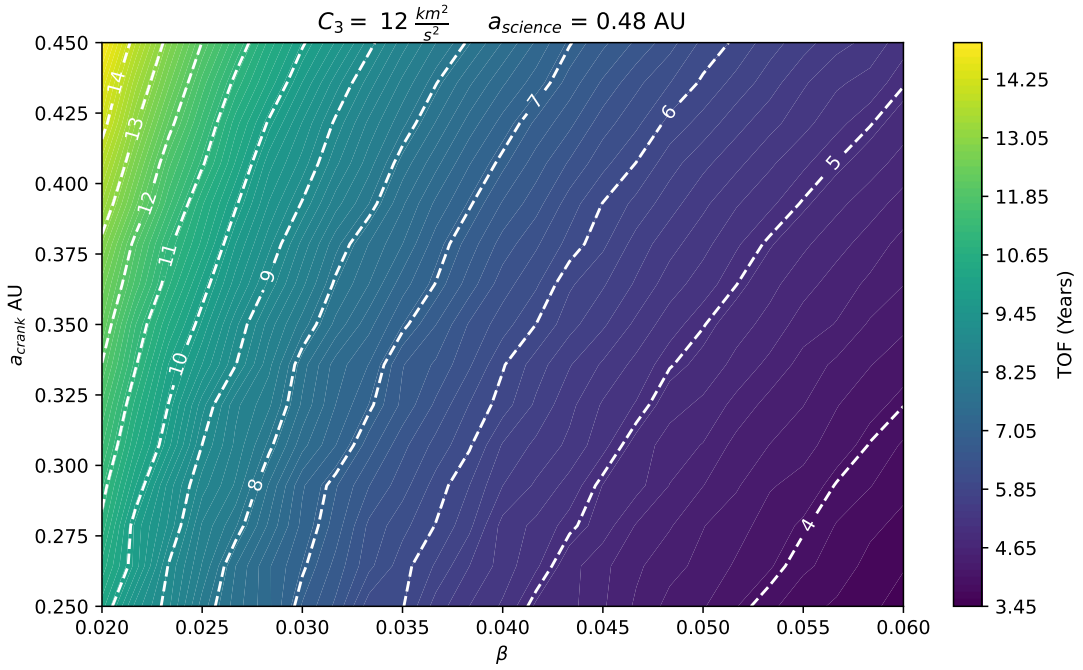

Figure 6: Overall TOF for Optimal Venus Flyby SPI Architecture, $C_3 = 12 \frac{km^2}{s^2}$

that multi-revolution low-thrust trajectories can have numerous local minima. Remarkably though, the Venus Flyby is improving TOF across all β and a_{crank} examined. Scanning left to right, it is evident that the Venus flyby has a greatest effect on small sail-craft, with up to a 17% TOF improvement for sails similar in size to Solar Cruiser ($\beta \approx .02$). However, this trend diminishes down to only roughly 12% for the largest sails examined.

Increasing the departure C_3 to 36 $\frac{km^2}{s^2}$ and calculating the optimal TOF for both architectures results in the TOF contour plots shown in fig. 8 and fig. 9. As one might expect, both architectures benefit from the increase in departure C_3, across all values of β and a_{crank}. However, as is evident from the percentage TOF improvement plot shown in fig. 10, increasing C_3 appears to benefit the standard SPI architecture more than the Venus flyby architecture. This is particularly evident at large β values and lower cranking radii, where the Venus flyby is only delivering 6% faster overall mission times as compared to 12% in the lower C_3 case.

CONCLUSION

In this work, a process was developed to generate time-optimal solar sail transfers for a Solar Polar Imager (SPI) mission. The standard mission architecture leveraging only the sail and Earth departure energy was compared to one including a Venus flyby across a range of feasible sail sizes. Results indicate that the Venus flyby mission architecture can offer significant improvements of 12% to 17% in overall TOF for low to moderate Earth departure energies. However, for larger sail sizes and higher C_3, the Venus flyby offers smaller improvements in TOF.

ACKNOWLEDGMENTS

This work was partially funded by NASA under Grant No. 80NSSC21K1871. The first author would also like to acknowledge the support of the National Science Foundation under Grant No.1645423. Any opinions, findings, and conclusions or recommendations expressed in this material are those of the authors and do not necessarily reflect the views of the National Science Foundation.

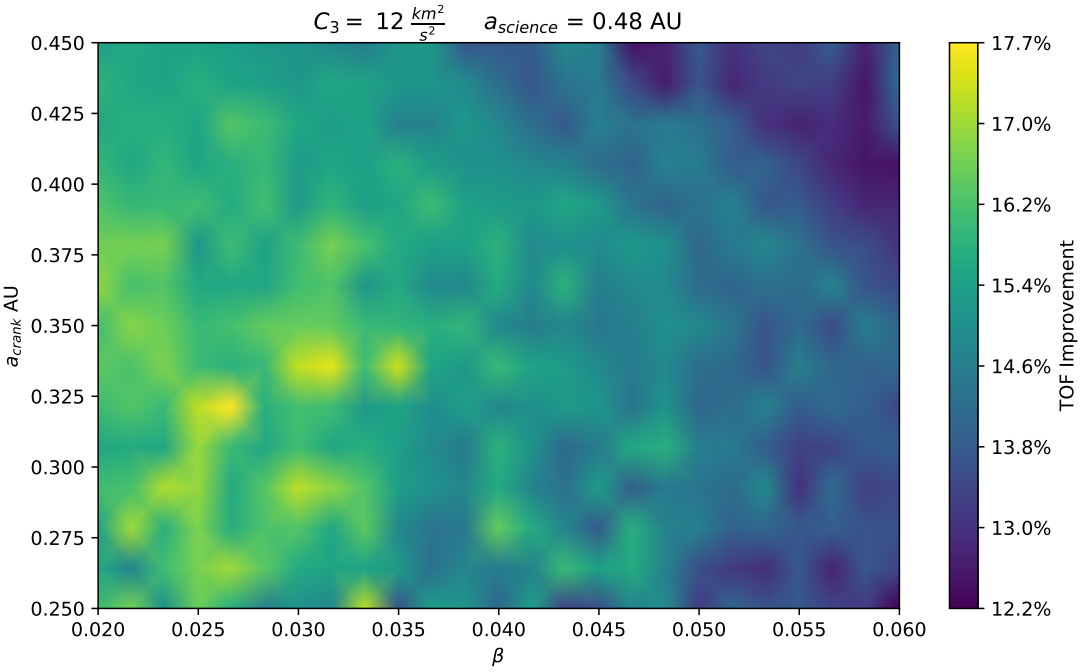

Figure 7: TOF Improvement of Venus Flyby SPI over Standard SPI, $C_3 = 12 \frac{km^2}{s^2}$

REFERENCES

[1] K. Kobayashi, L. Johnson, H. Thomas, S. McIntosh, D. McKenzie, J. Newmark, A. Heaton, J. Carr, M. Baysinger, Q. Bean, *et al.*, "The high inclination solar mission," *arXiv preprint arXiv:2006.03111*, 2020.

[2] K. Wenzel, R. Marsden, D. Page, and E. Smith, "The ULYSSES mission," *Astronomy and Astrophysics Supplement Series*, Vol. 92, 1992, p. 207.

[3] D. Alexander, A. Sandman, P. Liewer, J. Ayon, B. Goldstein, N. Murphy, M. Velli, L. Floyd, D. Moses, D. Socker, A. Vourlidas, G. Garbe, S. Suess, D. Hassler, A. Kosovichev, R. Mewaldt, M. Neugebauer, R. Ulrich, and T. Zurbuchen, "Solar Polar Imager: Observing Solar Activity from a New Perspective," Vol. 592, 08 2005, p. 663.

[4] T. Appourchaux, P. Liewer, M. Watt, D. Alexander, V. Andretta, F. Auchère, P. D'Arrigo, J. Ayon, T. Corbard, S. Fineschi, *et al.*, "POLAR investigation of the Sun—POLARIS," *Experimental Astronomy*, Vol. 23, No. 3, 2009, pp. 1079–1117.

[5] B. Wie, S. Thomas, M. Paluszek, and D. Murphy, "Propellantless aocs design for a 160-m, 450-kg sailcraft of the solar polar imager mission," *41st AIAA/ASME/SAE/ASEE Joint Propulsion Conference & Exhibit*, 2005, p. 3928.

[6] C. Sauer, "Solar sail trajectories for solar polar and interstellar probe missions," *Advances in the Astronautical Sciences Volume 103, Part I. Astrodynamics 1999*, Vol. 103, 01 2000, pp. 547–562.

[7] B. Dachwald, A. Ohndorf, and B. Wie, "Solar sail trajectory optimization for the solar polar imager (SPI) mission," *AIAA/AAS Astrodynamics Specialist Conference and Exhibit*, 2006, p. 6177.

[8] M. Macdonald, G. W. Hughes, C. R. McInnes, A. Lyngvi, P. Falkner, and A. Atzei, "Solar polar orbiter: a solar sail technology reference study," *Journal of Spacecraft and Rockets*, Vol. 43, No. 5, 2006, pp. 960–972.

[9] G. Mengali and A. A. Quarta, "Solar sail near-optimal circular transfers with plane change," *Journal of guidance, control, and dynamics*, Vol. 32, No. 2, 2009, pp. 456–463.

[10] A. A. Quarta and G. Mengali, "Solar sail missions to Mercury with Venus gravity assist," *Acta Astronautica*, Vol. 65, No. 3-4, 2009, pp. 495–506.

[11] M. Walker, "A set of modified equinoctial orbit elements," *Celestial mechanics*, Vol. 38, No. 4, 1986, pp. 391–392.

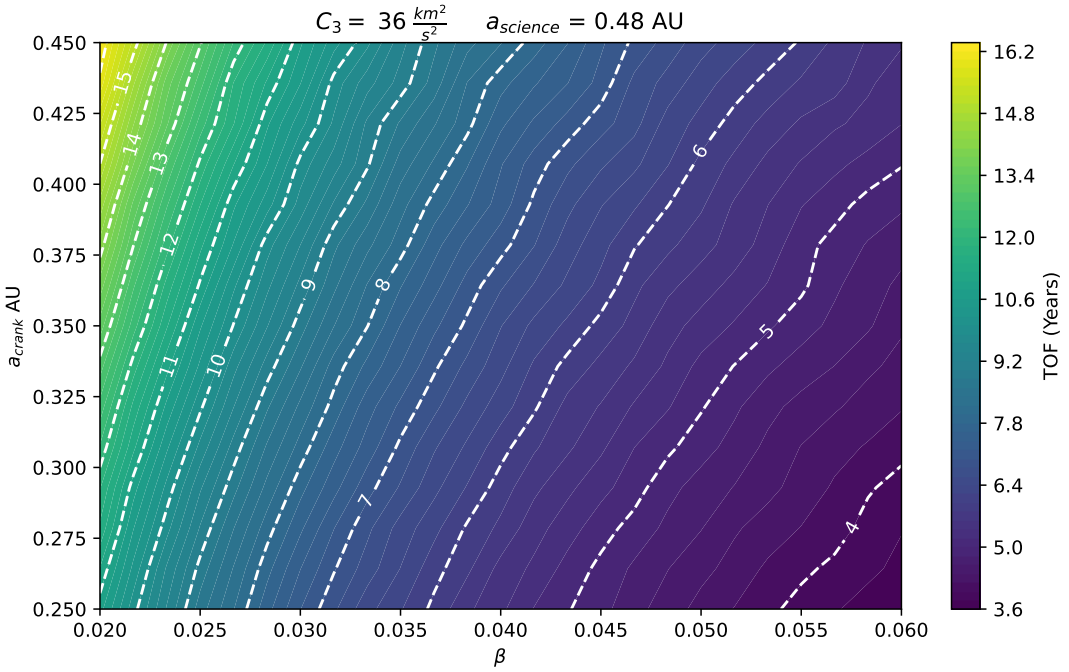

Figure 8: Overall TOF for Optimal Standard SPI Architecture, $C_3 = 36 \frac{km^2}{s^2}$

[12] J. L. Junkins and E. Taheri, "Exploration of alternative state vector choices for low-thrust trajectory optimization," *Journal of Guidance, Control, and Dynamics*, Vol. 42, No. 1, 2019, pp. 47–64.

[13] A. Heaton, N. Ahmad, and K. Miller, "Near earth asteroid scout thrust and torque model," *International Symposium on Solar Sailing (ISSS 2017)*, No. M17-5721, 2017.

[14] J. B. Pezent, R. Sood, A. Heaton, K. Miller, and L. Johnson, "Preliminary trajectory design for NASA's Solar Cruiser: A technology demonstration mission," *Acta Astronautica*, Vol. 183, 2021, pp. 134–140.

[15] L. Johnson, J. Everett, D. McKenzie, D. Tyler, D. Wallace, J. Newmark, D. Turse, M. Cannella, J. Wilson, and M. Feldman, "The NASA Solar Cruiser Mission-Solar Sail Propulsion Enabling Heliophysics Missions," *36th Annual Small Satellite Conference*.

[16] J. Everett, A. Heaton, A. Houin, and K. Miller, "An Integrated Software Architecture for Solar Cruiser Mission Design and Navigation," *2022 IEEE Aerospace Conference (AERO)*, IEEE, 2022, pp. 1–9.

[17] J. T. Betts and S. O. Erb, "Optimal low thrust trajectories to the moon," *SIAM Journal on Applied Dynamical Systems*, Vol. 2, No. 2, 2003, pp. 144–170.

[18] J. B. Pezent, J. Sikes, W. Ledbetter, R. Sood, K. C. Howell, and J. R. Stuart, "ASSET: Astrodynamics Software and Science Enabling Toolkit," *AIAA SCITECH 2022 Forum*, 2022, p. 1131, 10.2514/6.2022-1131.

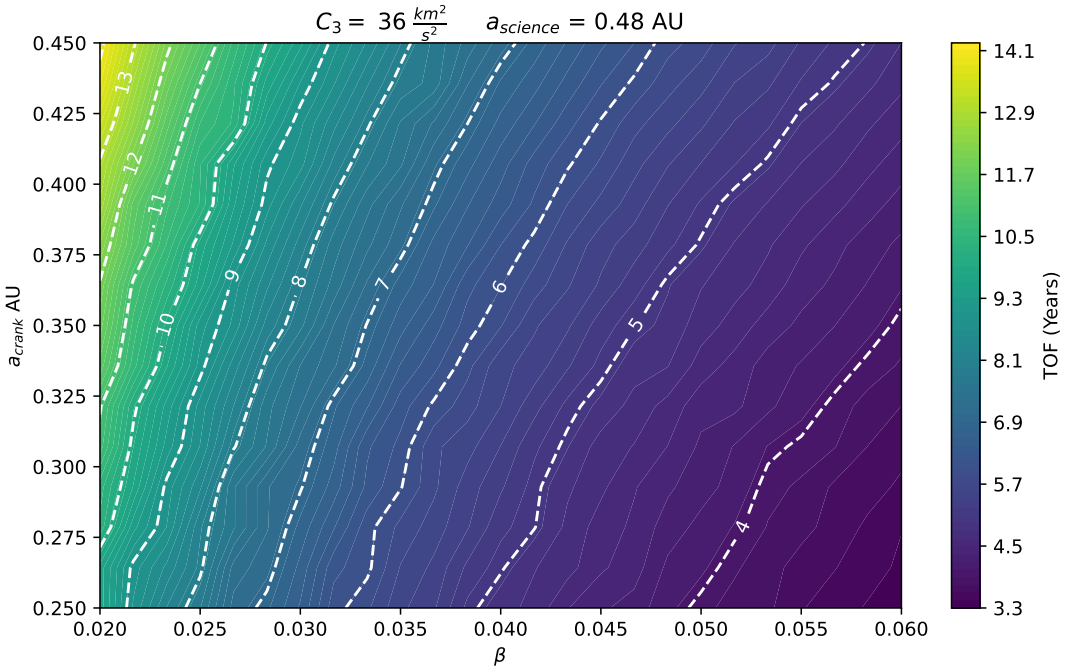

Figure 9: Overall TOF for Optimal Venus Flyby SPI Architecture, $C_3 = 36 \frac{km^2}{s^2}$

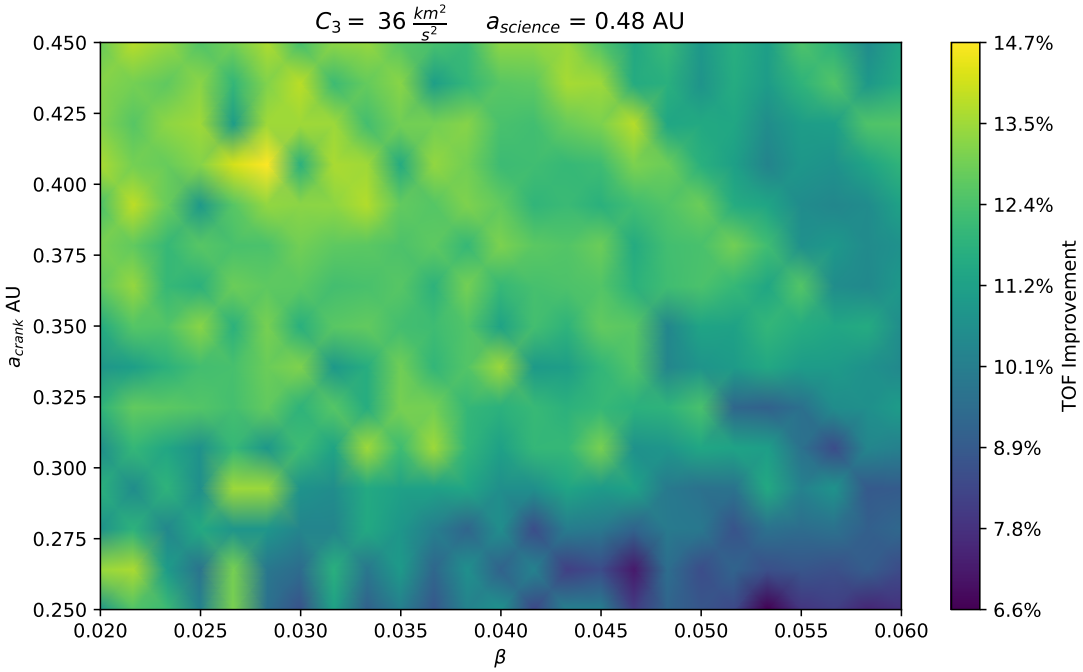

Figure 10: TOF Improvement of Venus Flyby SPI over Standard SPI, $C_3 = 36 \frac{km^2}{s^2}$